SEM Case Studies

J. Goldstein et al., *Scanning Electron Microscopy and X-Ray Microanalysis*,
https://doi.org/10.1007/978-1-4939-6676-9_15

15.1 Case Study: How High Is That Feature Relative to Another?

When studying the topographic features of a specimen, the microscopist has several useful software tools available. Qualitative stereomicroscopy provides a composite view from two images of the same area, prepared with different tilts relative to the optic axis, that gives a visual sensation of the specimen topography, as shown for a fractured galena crystal using the anaglyph method in Fig. 15.1 (software: Anaglyph Maker). The "3D Viewer" plugin in ImageJ-Fiji can take the same members of the stereo pair and render the three-dimensional surface, as shown in Fig. 15.2, which can then be rotated to "view" the surface from different orientations (Fig. 15.3).

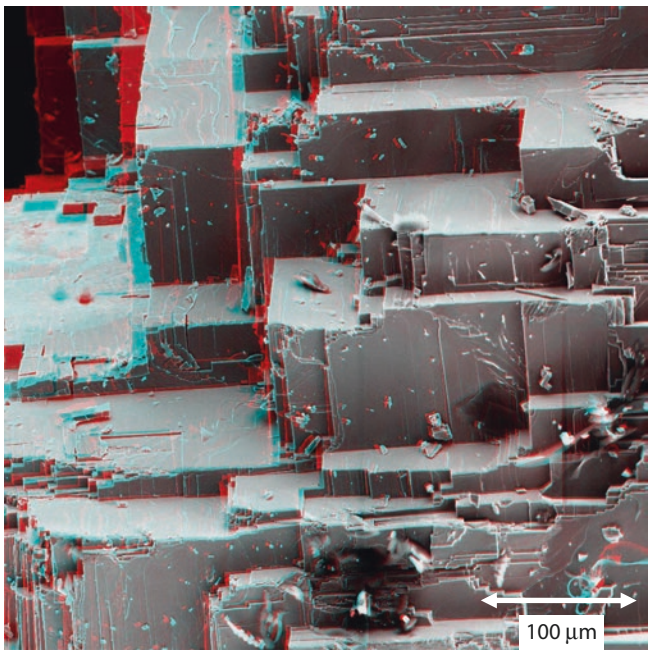

Fig. 15.1 Anaglyph stereo pair presentation (software: Anaglyph Maker), to be viewed with the red filter over the left eye. Sample: fractured galena; Everhart–Thornley detector(positive bias); $E_0 = 20$ keV

If the question is, How high is that feature relative to another?, as shown in Fig. 15.4 for the step height indicated by the yellow arrow, then the methodology of quantitative stereomicroscopy can be applied. First, a set of X-Y-coordinates is established by locating features common to both members of the stereo pair; for example, in Fig. 15.5a the red crosshair is placed on a feature in the lower surface which will define the origin of coordinates (0, 0). A feature is similarly identified in the upper surface, for example, the particle marked by the blue crosshair in Fig. 15.5a and the red arrow in Fig. 15.5b. The principle of the parallax measurement of the upper feature relative to the lower feature using these coordinate axes is illustrated in Fig. 15.5b, c. What is needed is the difference in the X-coordinates of the lower and upper reference features to determine the length of the X-vector from the measurement axes, which is the parallax for this feature. These measurements are conveniently made using the pixel coordinate feature in ImageJ-Fiji. By employing the expanded views presented in Fig. 15.6a, b for the left image, the individual pixels that define the reference points can be more readily seen, which improves the specificity of the feature location within the two images to ±1 pixel, minimizing this important source of measurement error. Having first calibrated the images using the "Set Scale" tool, the x-coordinate values from the pixel coordinate tool, from both the left and right images (with a tilt difference $\Delta\theta = 4^0$ with an estimated uncertainty of $\pm 1^0$), were used in the following calculations:

$$\text{Left image : X-vector length (red)} = 214.9\ \mu\text{m} - 137.8\ \mu\text{m} = 77.1\ \mu\text{m} \quad (15.1)$$

$$\text{Right image : X-vector length (blue)} = 187.9\ \mu\text{m} - 121.0\ \mu\text{m} = 66.9\ \mu\text{m} \quad (15.2)$$

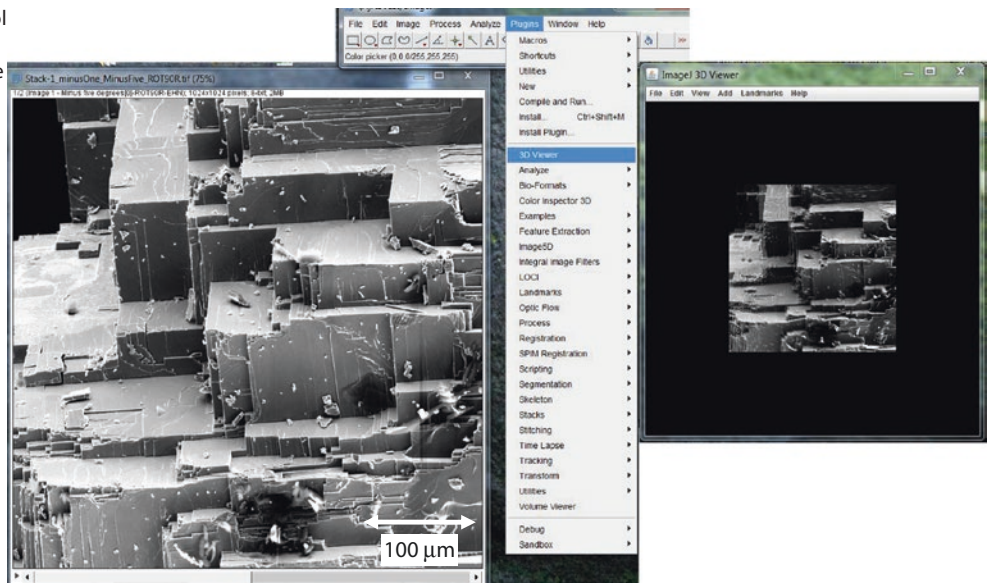

Fig. 15.2 "3D Viewer" plugin tool in ImageJ-Fiji operating on the same stereo pair presented as a two-image stack to create a rendering of the object surface

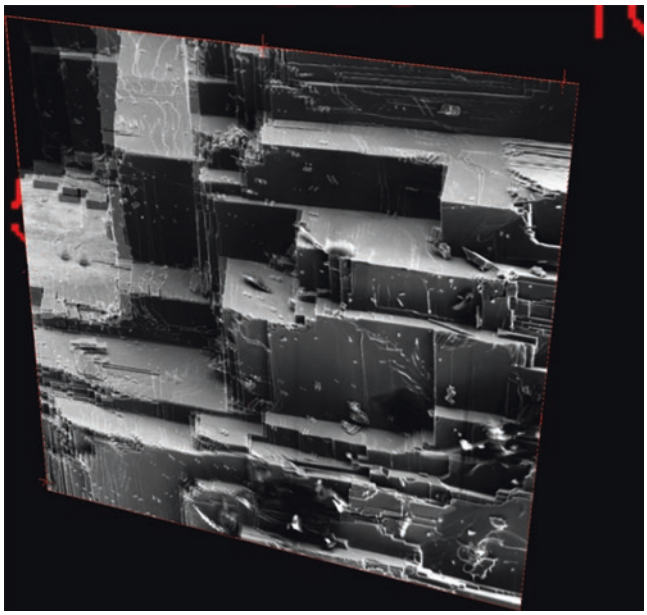

Fig. 15.3 "3D Viewer" rotation of the rendered surface

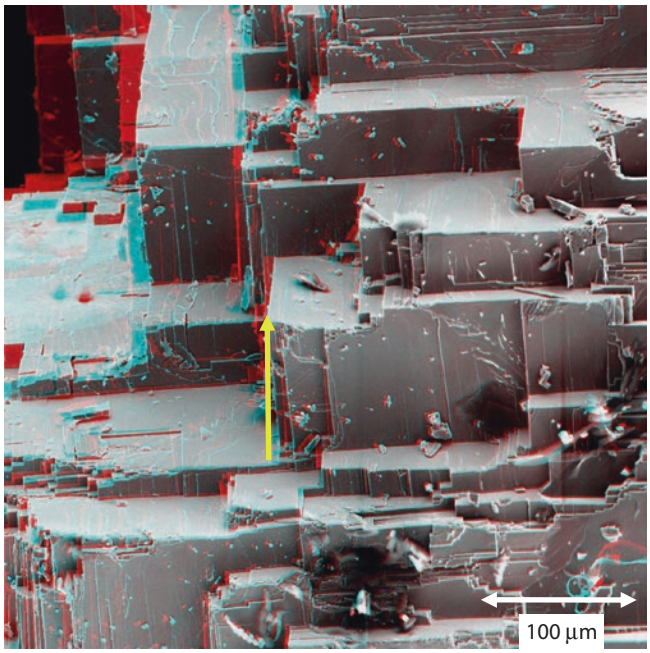

Fig. 15.4 Step height to be measured (*yellow arrow*)

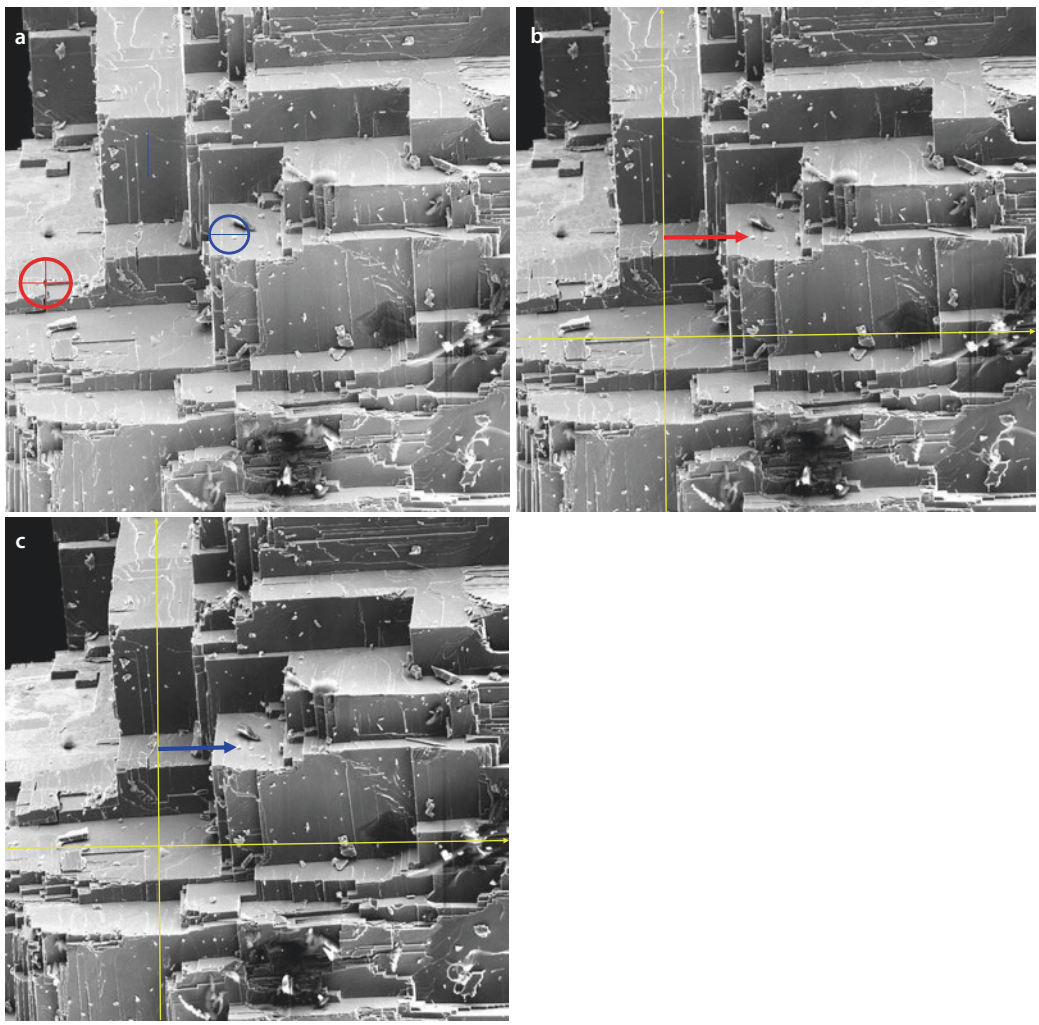

Fig. 15.5 **a** Selection of lower (*red crosshair*) and upper (*blue crosshair*) features that lie on the lower and upper surfaces of the step to be measured. **b** Coordinate system established in the left-hand image relative to the lower surface feature. **c** Coordinate system established in the right-hand image relative to the lower surface feature

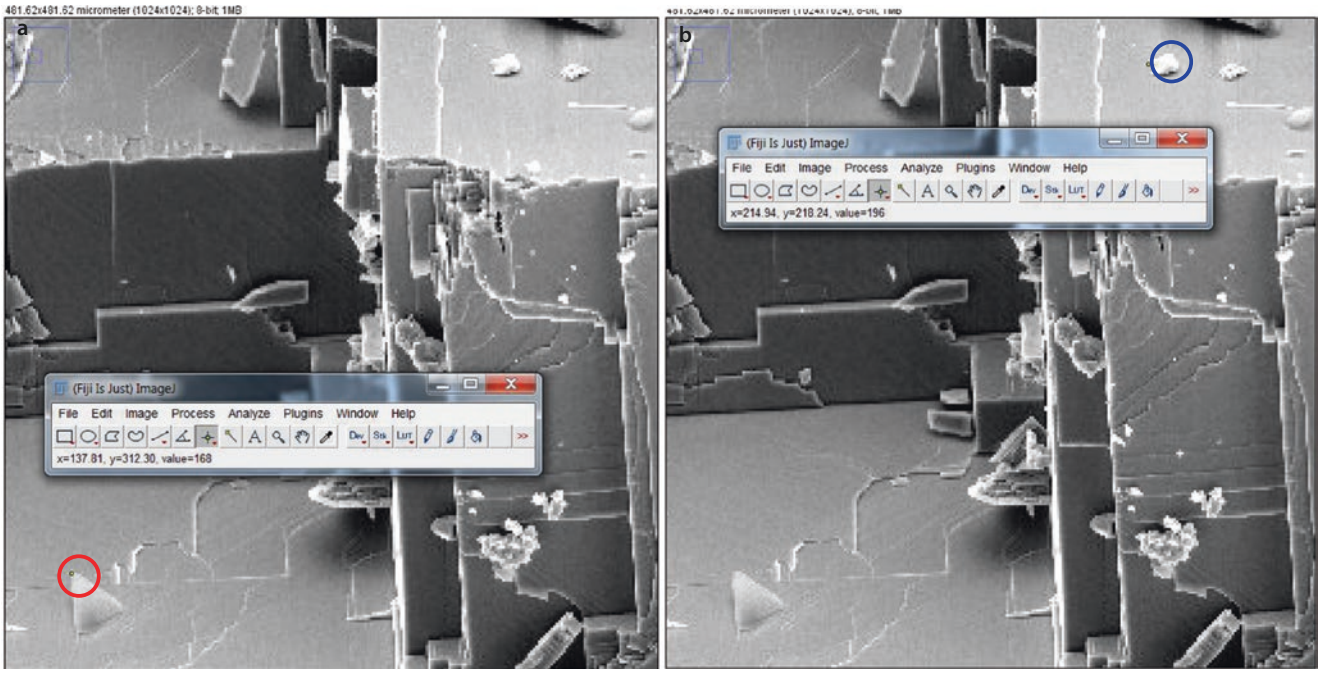

Fig. 15.6 **a** Use of the single pixel measurement feature in ImageJ-Fiji to select the reference pixel (center of the *red circle*) on the lower surface feature. **b** Use of the single pixel measurement feature in ImageJ-Fiji to select the reference pixel (center of the *blue circle*) on the upper surface feature

Parallax = $X_{\text{Left}} - X_{\text{right}} = 77.1\ \mu\text{m} - 66.9\ \mu\text{m} = 10.2\ \mu\text{m}$ (Note that the parallax has a positive sign, so the feature is *above* the reference point.)

$$Z = P/\left[2\sin(\Delta\theta)/2\right] = 10.2\ \mu\text{m}/\left[2\sin\left(4^0/2\right)\right] = 146.1\ \mu\text{m} \pm 6\ \% \quad (15.3)$$

Thus, the step represented by the yellow arrow in Fig. 15.4 is 146.1 µm ± 6 % above the origin of the yellow arrow. The estimated uncertainty has two major components: an uncertainty of 0.1^0 in the tilt angle difference contributes an uncertainty of ± 5 % to the calculated step height. A ± 1 pixel uncertainty in selecting the same reference pixels for the lower and upper features in both images contributes ± 4 % to the calculated step height.

15.2 Revealing Shallow Surface Relief

Surfaces with topographic structures that create shallow surface relief a few tens to hundreds of nanometers above the general surface provide special challenges to SEM imaging: (1) Shallow topography creates only small changes in the electron interaction volume and in the resulting emitted secondary electron (SE) and backscattered (BSE) signals as the beam is scanned across a feature, resulting in low contrast. (2) The strongest changes in the emitted signals from the weak topographic features will be found in the trajectory effects of the BSE rather than in the numbers of the BSE or SE signals, so that an appropriate detector should be chosen that emphasizes the BSE trajectory component of topographic contrast. (3) Because the shallow relief is likely to provide very few "clues" as to the sense of the topography, it is critical to establish a condition of top lighting so that the sense of the local topography can be more easily determined. (4) Establishing the visibility of low contrast requires exceeding a high threshold current, so that careful control of beam current will be necessary. (5) The displayed image must be contrast manipulated to render the low contrast visible to the observer, which may be challenging if other sources of contrast are present.

An example of the shallow surface relief imaging problem is illustrated by a highly polished specimen with a microstructure consisting of large islands of Fe_3C (cementite) in pearlite (interpenetrating lath-like structures of Fe_3C and an iron-carbon solid solution). The strategy for obtaining a useful image of this complex specimen is based on the realization that the weak contrast from the shallow topography will be maximized with the BSE signal detected with a detector with a small solid angle of collection placed asymmetrically relative to the specimen and with a shallow detector elevation angle above the surface to produce the effect of oblique illumination. The small solid angle means that most BSE trajectories not directed into the detector will be lost, which actually increases the contrast. The asymmetric placement and shallow elevation angle ensures that the apparent illumination will come from a source that skims the surface, creating the effect of oblique illumination which creates strong shadows. The Everhart–Thornley (E–T) detector when

biased negatively to reject SEs becomes a small solid angle BSE detector with these characteristics. The E–T detector is typically mounted so as to produce a shallow elevation angle relative to a specimen plane that is oriented perpendicular to the incident beam (0° tilt for a planar specimen). Before proceeding with the imaging campaign, the relative position of the E–T detector is confirmed to be at the 12-o'clock position in the image by using the "scan rotation" function and a specimen with known topography.

Figure 15.7 shows an image of the iron-carbon microstructure with the negatively biased E–T detector placed at the top of the image. A high beam current (10 nA) and a long dwell time (256 µs per pixel) were used to establish the visibility of low contrast. The displayed contrast was expanded by first ensuring that the histogram of gray levels in the raw image was centered at mid-range and did not clip at the black or white ends. The "brightness" and "contrast" functions in ImageJ-Fiji were used to spread the input BSE intensity levels over a larger gray-scale output range. The contrast can be interpreted as follows: With the apparent illumination established as coming from the top of the image, bright edges must therefore be facing upward, and conversely, dark edges must be facing away. Thus, the topography of the Fe_3C islands can be seen to project slightly above the general surface. This situation occurs because the Fe_3C is harder than the iron-carbon solid solution, so that when this material is polished, the softer iron-carbon solid solution erodes slightly faster than the harder Fe_3C phase, which then stands in slight relief above the iron-carbon solid solution.

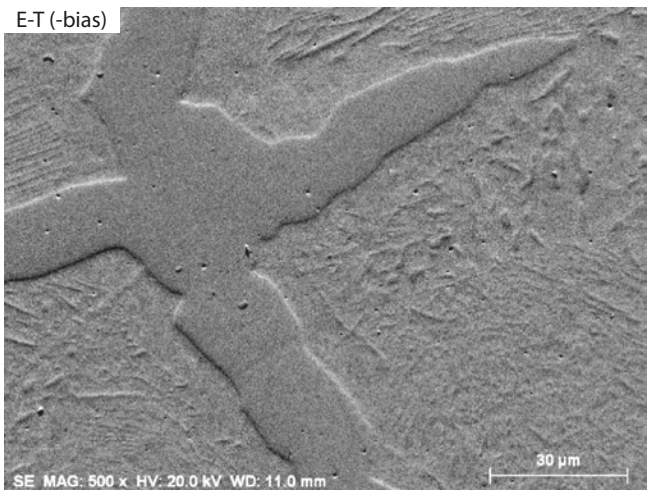

Fig. 15.7 Highly polished iron-carbon specimen imaged at $E_0 = 20$ keV and $I_p = 10$ nA with the negatively biased E–T detector. Image dimensions: 140 × 105 µm (Bar = 30 µm)

When this same field of view is imaged with the E–T detector positively biased, Fig. 15.8a, the same general contrast is seen, but there are significant differences in the fine-scale details. Several of these differences are highlighted in Fig. 15.8b. (1) It is much easier to discern the numerous small pits (e.g., yellow circles) in the E–T(positive bias) image because of the strong "bright edge" effects that manifest along the lip of each hole. (2) There are small objects (e.g., blue circles) which appear in the E–T(negative bias) image but which appear anomalously dark in the E–T(positive bias) image. These objects are likely to be non-conducting oxide inclusions that are charging positively, which decreases SE collection.

When this same field of view is imaged with the annular semiconductor BSE detector (sum mode, A + B) which provides apparent uniform, symmetric illumination along the beam, as shown in Fig. 15.9, the contrast from the shallow topography of the edges of the Fe_3C islands is entirely lost, whereas the compositional contrast (atomic number contrast) between the Fe_3C islands and the iron-carbon solid solution and Fe_3C lamellae is much more prominent.

Finally, when the BSE difference mode (A − B) mode is used, Fig. 15.10, the atomic number contrast is suppressed and the topographic contrast is enhanced. Note that the features highlighted in the blue circles in Fig. 15.8b are almost completely lost.

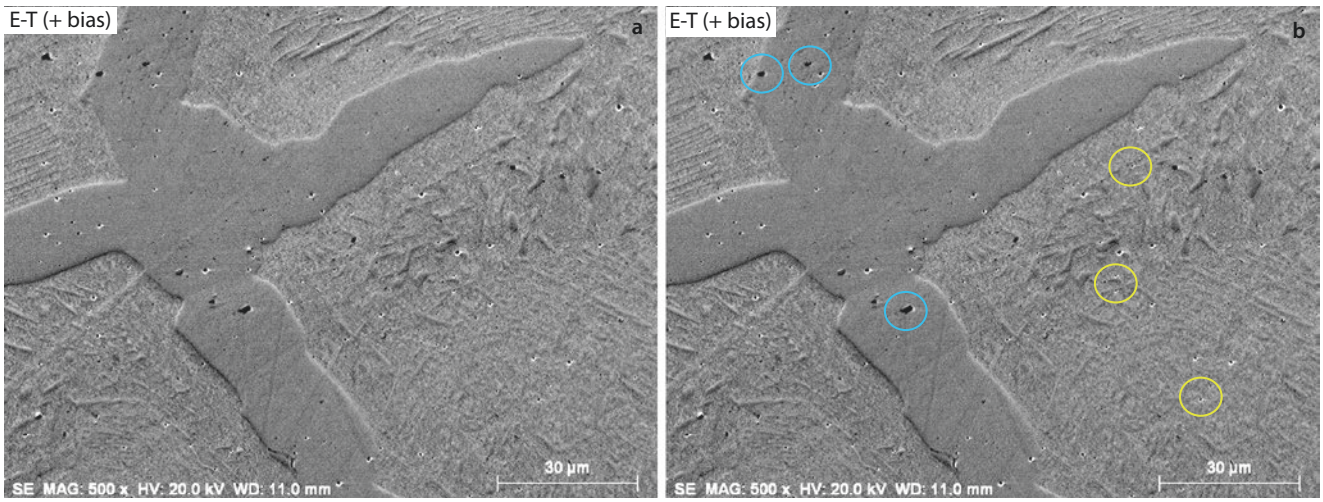

Fig. 15.8 **a** Same area imaged with a positively biased E–T detector. **b** Selected features highlighted for comparison

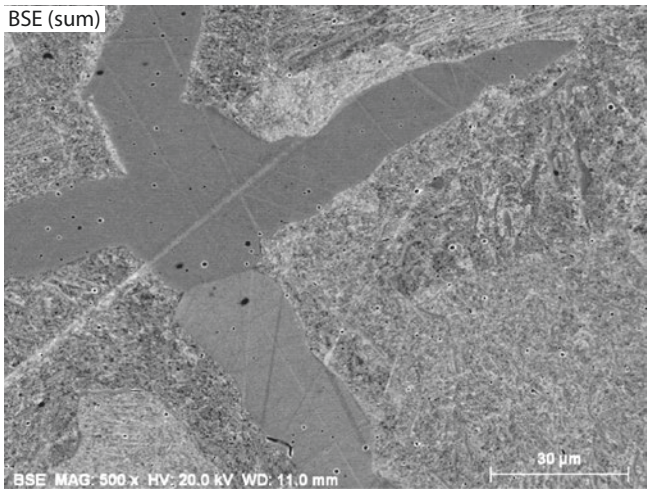

Fig. 15.9 Same area imaged with an annular semiconductor BSE detector (sum mode, A + B)

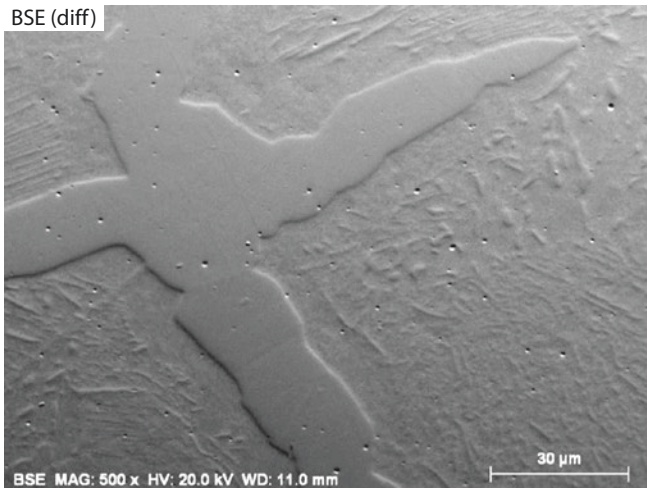

Fig. 15.10 Same area imaged with an annular semiconductor BSE detector (difference mode, A − B)

15.3 Case Study: Detecting Ink-Jet Printer Deposits

Ink-jet printing was used to deposit controlled quantities of reagents in individual droplets onto a polished carbon substrate in a project to create standards and test materials for instrumental microanalysis techniques such as secondary ion mass spectrometry. The spatial distribution of the dried deposits was of interest, as well as any heterogeneity within the deposits, which required elemental microanalysis.

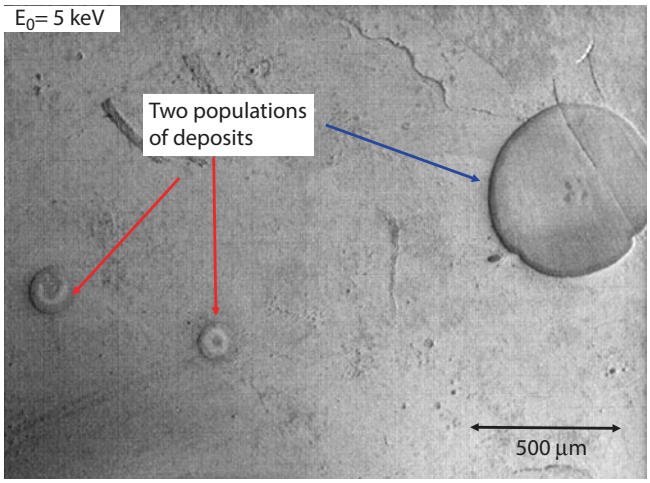

Fig. 15.11 SEM-ET (positive bias) image of ink-jet deposits on a polished carbon substrate with $E_0 = 5$ keV; 32 µs/pixel = 25 s frame time

The first critical step, detecting the ink-jet printed spots, proved to be a challenge because of the low contrast created by the thin, low mass deposit. Employing a low beam energy, $E_0 \leq 5$ keV, and secondary electron imaging using the positively biased Everhart–Thornley detector, maximized the contrast of the deposits, enabling detection of two different size classes of deposits, as seen in Fig. 15.11. When the beam energy was increased to enable the required elemental X-ray microanalysis, the visibility of the deposits diminished rapidly. Even with $E_0 = 10$ keV, which is the lowest practical beam energy to excite the K-shell X-rays of the transition metals, and a beam current of 10 nA, the deposits were not visible in high scan rate ("flicker free") imaging that is typically used when surveying large areas of a specimen to find features of interest. To reliably relocate the deposits at higher beam energy, a successful imaging strategy required both high beam current, for example, 10 nA, and long frame time, several seconds or longer, as shown in Fig. 15.12a–h. In this image series, the deposits are not visible at the shortest frame time of 0.79 s, which is similar to the visual persistence of a rapid scanned image. The class of approximately 100-µm diameter deposits is fully visible in the 6.4 s/frame image. As the frame time is successively extended to 100 s, additional features of progressively lower contrast become visible with each increase in frame time.

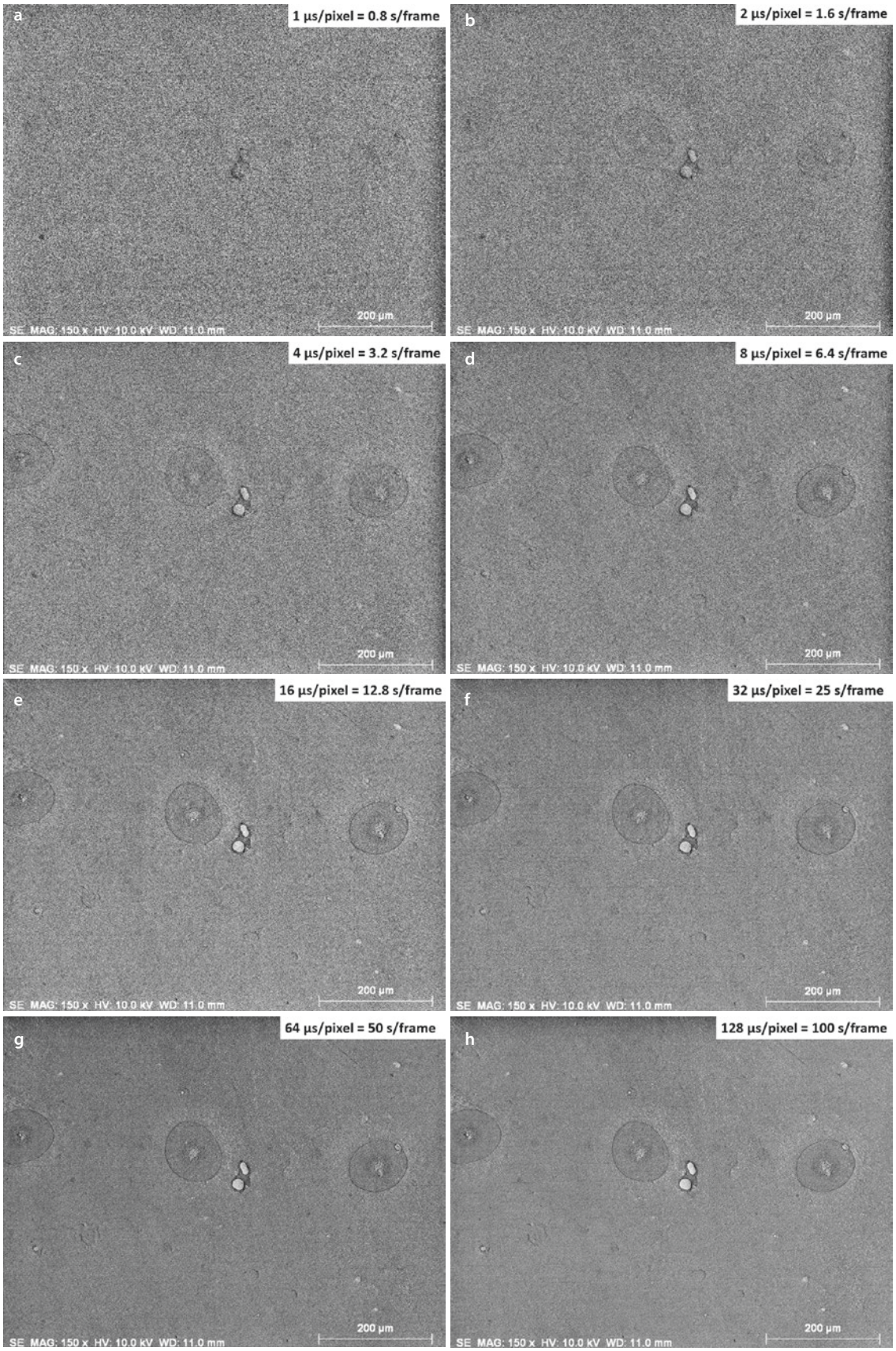

Fig. 15.12 **a** SEM-ET (positive bias) image of ink-jet deposits on a polished carbon substrate with $E_0 = 10$ keV: 1 µs/pixel = 0.8 s frame time. **b** 2 µs/pixel = 1.6 s frame time. **c** 4 µs/pixel = 3.2 s frame time. **d** 8 µs/pixel = 6.4 s frame time. **e** 16 µs/pixel = 12.8 s frame time. **f** 32 µs/pixel = 25 s frame time. **g** 64 µs/pixel = 50 s frame time. **h** 64 µs/pixel = 100 s frame time